

Observation of spontaneous polarization misalignments in periodically poled crystals using second-harmonic generation microscopy

Yu-Yi Tzeng,¹ Zong-Yan Zhuo,¹ Ming-Yin Lee,¹ Chien-Sheng Liao,¹ Pei-Chun Wu,³ Chin-Jie Huang,³ Ming-Che Chan,² Tzu-Ming Liu,³ Yen-Yin Lin,^{4,5,6} and Shi-Wei Chu^{1,6,*}

¹Department of Physics, National Taiwan University, No. 1, Sec. 4, Roosevelt Rd, Taipei 10617, Taiwan

²Institute of Imaging and Biomedical Photonics, National Chiao-Tung University, Tainan, Taiwan

³Institute of Biomedical Engineering, National Taiwan University, Taipei, Taiwan

⁴Institute of Photonics Technologies, Department of Electrical Engineering, National Tsing-Hua University, Hsinchu, Taiwan

⁵Brain Research Center, National Tsing-Hua University, Hsinchu, Taiwan

⁶These authors contribute equally to this work

*swchu@phys.ntu.edu.tw

Abstract: Periodically poled crystal (PPC) is a key component for nonlinear optical applications. Its poling quality relies largely on successful domain inversion and the alignment of spontaneous polarization (SP) vectors in each domain. Here we report the unexpected observation of bulk second harmonic generation (SHG) in PPC when excitation propagating along its optical axis. Based on its tensorial nature, SHG is highly sensitive to the orientation of SP, and therefore the misalignment of SP in each domain of PPC can be revealed noninvasively by SHG microscopy. This nonlinear imaging modality provides optical sectioning capability with 3D sub-micrometer resolution, so it will be useful for *in situ* investigation of poling quality in PPC.

©2011 Optical Society of America

OCIS codes: (160.3730) Lithium niobate; (180.4315) Nonlinear microscopy; (190.2620) Harmonic generation and mixing; (190.4400) Nonlinear optics, materials.

References and links

1. M. M. Fejer, G. A. Magel, D. H. Jundt, and R. L. Byer, "Quasi-phase-matched second harmonic generation: tuning and tolerances," *IEEE J. Quantum Electron.* **28**(11), 2631–2654 (1992).
2. M. Yamada, N. Nada, M. Saitoh, and K. Watanabe, "First-order quasi-phase matched LiNbO₃ waveguide periodically poled by applying an external field for efficient blue second-harmonic generation," *Appl. Phys. Lett.* **62**(5), 435–436 (1993).
3. J. Wang, J. Q. Sun, C. Lou, and Q. Z. Sun, "Experimental demonstration of wavelength conversion between ps-pulses based on cascaded sum- and difference frequency generation (SFG+DFG) in LiNbO₃ waveguides," *Opt. Express* **13**(19), 7405–7414 (2005).
4. Y. J. Ding, Y. Jiang, G. Xu, and I. B. Zotova, "Review of recent efforts on efficient generation of monochromatic THz pulses based on difference-frequency generation," *Laser Phys.* **20**(5), 917–930 (2010).
5. Y. S. Lee, T. Meade, V. Perlin, H. Winful, T. B. Norris, and A. Galvanauskas, "Generation of narrow-band terahertz radiation via optical rectification of femtosecond pulses in periodically poled lithium niobate," *Appl. Phys. Lett.* **76**(18), 2505–2507 (2000).
6. A. Dubietis, R. Butkus, and A. P. Piskarskas, "Trends in chirped pulse optical parametric amplification," *IEEE J. Sel. Top. Quantum Electron.* **12**(2), 163–172 (2006).
7. Y. W. Tzeng, Y. Y. Lin, C. H. Huang, J. M. Liu, H. C. Chui, H. L. Liu, J. M. Stone, J. C. Knight, and S. W. Chu, "Broadband tunable optical parametric amplification from a single 50 MHz ultrafast fiber laser," *Opt. Express* **17**(9), 7304–7309 (2009).
8. T. Ellenbogen, N. Voloch-Bloch, A. Ganany-Padowicz, and A. Arie, "Nonlinear generation and manipulation of Airy beams," *Nat. Photonics* **3**(7), 395–398 (2009).
9. D. Janner, D. Tulli, M. Garcia-Granda, M. Belmonte, and V. Pruneri, "Micro-structured integrated electro-optic LiNbO₃ modulators," *Laser Photon. Rev.* **3**(3), 301–313 (2009).
10. Y. Y. Lin, S. T. Lin, G. W. Chang, A. C. Chiang, Y. C. Huang, and Y. H. Chen, "Electro-optic periodically poled lithium niobate Bragg modulator as a laser Q-switch," *Opt. Lett.* **32**(5), 545–547 (2007).

11. I. E. Barry, G. W. Ross, P. G. R. Smith, R. W. Eason, and G. Cook, "Microstructuring of lithium niobate using differential etch-rate between inverted and non-inverted ferroelectric domains," *Mater. Lett.* **37**(4-5), 246–254 (1998).
12. M. J. Missey, S. Russell, V. Dominic, R. G. Batchko, and K. L. Schepler, "Real-time visualization of domain formation in periodically poled lithium niobate," *Opt. Express* **6**(10), 186–195 (2000).
13. V. Gopalan, Q. X. Jia, and T. E. Mitchell, "In situ video observation of 180° domain kinetics in congruent LiNbO₃ crystals," *Appl. Phys. Lett.* **75**(16), 2482–2484 (1999).
14. F. Saurenbach and B. D. Terris, "Imaging of ferroelectric domain-walls by force microscopy," *Appl. Phys. Lett.* **56**(17), 1703–1705 (1990).
15. R. Lüthi, H. Haefke, K. P. Meyer, E. Meyer, L. Howald, and H. J. Guntherodt, "Surface and domain-structures of ferroelectric-crystals studied with scanning force microscopy," *J. Appl. Phys.* **74**(12), 7461–7471 (1993).
16. G. Rosenman, A. Skliar, I. Lareah, N. Angert, M. Tseitlin, and M. Roth, "Observation of ferroelectric domain structures by secondary-electron microscopy in as-grown KTiOPO₄ crystals," *Phys. Rev. B Condens. Matter* **54**(9), 6222–6226 (1996).
17. Z. W. Hu, P. A. Thomas, and J. Webjorn, "High-resolution x-ray characterization of periodically domain-inverted nonlinear-optical crystals," *J. Phys. D Appl. Phys.* **28**(4A), A189–A194 (1995).
18. F. Kahmann, R. Matull, R. A. Rupp, and J. Seglins, "Polarization topography in photorefractive ferroelectrics," *Europhys. Lett.* **13**(5), 405–410 (1990).
19. V. Grubsky, S. Maccormack, and J. Feinberg, "All-optical three-dimensional mapping of 180° domains hidden in a BaTiO₃ crystal," *Opt. Lett.* **21**(1), 6–8 (1996).
20. V. Dierolf and C. Sandmann, "Inspection of periodically poled waveguide devices by confocal luminescence microscopy," *Appl. Phys. B-Lasers Opt.* **78**(3-4), 363–366 (2004).
21. J. Harris, G. Norris, and G. McConnell, "Characterisation of periodically poled materials using nonlinear microscopy," *Opt. Express* **16**(8), 5667–5672 (2008).
22. S. I. Bozhevolnyi, J. M. Hvam, K. Pedersen, F. Laurell, H. Karlsson, T. Skettrup, and M. Belmonte, "Second-harmonic imaging of ferroelectric domain walls," *Appl. Phys. Lett.* **73**(13), 1814–1816 (1998).
23. M. Flörshheimer, R. Paschotta, U. Kubitscheck, C. Brillert, D. Hofmann, L. Heuer, G. Schreiber, C. Verbeek, W. Sohler, and H. Fuchs, "Second-harmonic imaging of ferroelectric domains in LiNbO₃ with micron resolution in lateral and axial directions," *Appl. Phys. B-Lasers Opt.* **67**(5), 593–599 (1998).
24. Y. Sheng, A. Best, H. J. Butt, W. Krolikowski, A. Arie, and K. Koynov, "Three-dimensional ferroelectric domain visualization by Cerenkov-type second harmonic generation," *Opt. Express* **18**(16), 16539–16545 (2010).
25. Y. Uesu, H. Yokota, S. Kawado, J. Kaneshiro, S. Kurimura, and N. Kato, "Three-dimensional observations of periodically poled domains in a LiTaO₃ quasiphase matching crystal by second harmonic generation tomography," *Appl. Phys. Lett.* **91**(18), 182904 (2007).
26. J. Kaneshiro, Y. Uesu, and T. Fukui, "Visibility of inverted domain structures using the second harmonic generation microscope: comparison of interference and non-interference cases," *J. Opt. Soc. Am. B* **27**(5), 888–894 (2010).
27. S.-C. Pei, T.-S. Ho, C.-C. Tsai, T.-H. Chen, Y. Ho, P.-L. Huang, A. H. Kung, and S.-L. Huang, "Non-invasive characterization of the domain boundary and structure properties of periodically poled ferroelectrics," *Opt. Express* **19**(8), 7153–7160 (2011).
28. Z. Y. Zhuo, C. S. Liao, C. H. Huang, J. Y. Yu, Y. Y. Tzeng, W. Lo, C. Y. Dong, H. C. Chui, Y. C. Huang, H. M. Lai, and S. W. Chu, "Second harmonic generation imaging - a new method for unraveling molecular information of starch," *J. Struct. Biol.* **171**(1), 88–94 (2010).
29. J.-Y. Yu, C.-S. Liao, Z.-Y. Zhuo, C.-H. Huang, H.-C. Chui, and S.-W. Chu, "A diffraction-limited scanning system providing broad spectral range for laser scanning microscopy," *Rev. Sci. Instrum.* **80**(11), 113704 (2009).
30. Y. Saito, M. Kobayashi, D. Hiraga, K. Fujita, S. Kawano, N. I. Smith, Y. Inouye, and S. Kawata, "z-Polarization sensitive detection in micro-Raman spectroscopy by radially polarized incident light," *J. Raman Spectrosc.* **39**(11), 1643–1648 (2008).

1. Introduction

By changing the orientation of spontaneous polarization (SP) vector in ferroelectric crystals at fixed intervals, periodically poled crystals (PPCs) have been proven to be one of the most useful materials in nonlinear optics due to its high conversion efficiency from quasi-phase-matching. PPCs have been applied to enhance various second-order nonlinear optical interactions, including second harmonic generation (SHG) [1, 2], sum/difference frequency generation [3, 4], optical rectification [5], and optical parametric amplification [6, 7], etc, covering wavelengths from ultraviolet to terahertz regime. Patterns of PPCs are artificial and engineerable; thus PPCs have been used not only to study novel light-matter interactions [8], but also to increase bandwidth and lower down switching voltage in electro-optical modulators [9], with applications in laser Q-switch [10]. In general, the performance of PPC depends strongly on the poling quality so a method that is capable of characterizing the microstructures inside PPCs and checking its poling quality is highly desirable.

For many years, wet etching processes were adopted to reveal domain structures and period duty cycle [11], but the orientation alignment of SP inside PPCs cannot be unraveled by this invasive approach. Early imaging attempts to visualize such domains utilize bright field microscopies to observe scattering and monitor refractive index changes in the domain walls using crossed polarizers [12] and electro-optic imaging modifications [13] respectively. Other than optical microscopies, atomic force microscopy [14, 15], scanning electron microscopy [16], and x-ray diffraction technique [17] have also been applied for non-destructive imaging of PPCs. But these techniques lack three-dimensional resolution and provide little information of internal structures. More recently, 3D microscopy techniques, such as refractive coupling method [18, 19], confocal laser scanning microscopy [20], two-photon luminescence microscopy [21], SHG microscopy/interferometry [22–26], and very recently, optical coherence tomography [27] were adopted to study PPC. Sub- μm resolution of 3D domain structures has been achieved with these scanning microscopies. Nevertheless, luminescence-based techniques required specific doping of the media, strongly limiting their applications. SHG imaging, on the other hand, provides intrinsic contrast of the domains, as well as sensitivity on molecular axis from polarization anisotropy [28] that is critical when characterizing the domain. However previous SHG imaging studies on PPC are either concentrated on non-interferometric SHG from crystal interface and domain boundaries [22–24], or involved in complex experimental setup for interferometric SHG [25, 26]. In this paper we observed SHG from both domain boundaries and within the poled/non-poled domains based on simple non-interferometric imaging. We will demonstrate that the variation of SHG intensities in non-poled domains can be used as a quantitative indicator of poling quality.

2. Experimental setup

Figure 1 shows the schematics of our experimental setup. The instrumental detail can be found in [29], except that a commercial scanner is used alternatively. In brief, the excitation source is an ultrafast fiber laser (Uranus 005-500-INS, PolarOnyx, CA) with a wavelength of 1040 nm, a pulse width of 500 fs, a repetition rate of 48 MHz, and the maximal average power exceeding 5 W. However, 10 mW of average power is more than adequate to generate SHG images, and no photodamage is found after continuous observation. The laser is coupled into a commercial scanning microscope (FV300, Olympus, Japan), and is focused on the sample by an objective (UPLSAPO 20X, Olympus) with 0.75 numerical aperture (NA). The laser polarization lies in x - y plane at the focal plane, and the use of a mid-NA objective prevents depolarization. Linearly polarized laser is used and its polarization is controlled by a half-wave plate. The SHG signal is forward collected by a NA 0.9 condenser, and is measured by a photomultiplier tube. The spectral purity of SHG detection is ensured by insertion of an interference filter (F10-520, CVI Melles Griot) and a color filter (BG39, Schott) in front of the photomultiplier tube. Three-dimensional images are acquired by raster scanning in the x - y plane plus precise sample movement along the z -axis.

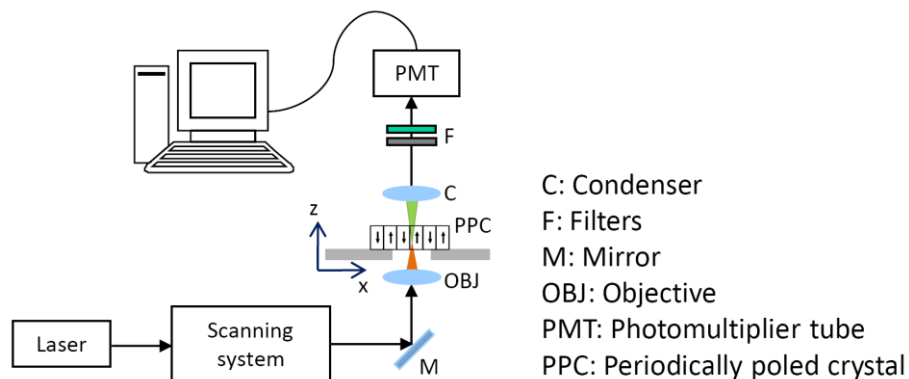


Fig. 1. Schematic of the scanning SHG microscope.

3. Periodically poled lithium niobate (PPLN) crystals

The samples are periodically poled lithium niobate (PPLN) crystals, which are one of the most popular PPCs for nonlinear conversion. Congruent LN substrates are z-cut 3-inch wafers from Crystal Technology Inc. In our fabrication procedures, grating patterns at +z surface are defined by standard lithographic processes, and the photoresist layer insulates the non-poled regions. The photoresist trenches at +z surface are filled with liquid electrolyte consisting of LiCl in deionized water. The dielectric properties of insulator layer are sensitive to hard-baking processes of photoresist, so quality control of PPCs is relatively complex. Here, in order to observe the domain structures, the excitation source is sent through the optical axis (z-axis), as shown in Fig. 1. If the SP of the PPLN crystals is aligned to the original crystal axis of blank wafer (z-axis), the incident laser are all ordinary waves and no phase matching condition can be achieved. Furthermore, there is no corresponding second-order nonlinear dipole in LN which can provide *ooo* interaction; As a result, no bulk SHG is expected under this geometry and SHG signal should only be observed from domain boundaries.

We have used multiple PPLN samples for SHG microscopy observation. All samples are designed with a 50% duty cycle. The SHG imaging results of three PPLN samples with different poling qualities will be presented in the following section. We will start with a well-poled sample to examine normal SHG responses in PPLN, and then characterize SHG images in poorly-poled samples. The first one is a well-poled 500- μm thick PPLN with a $\sim 70\text{-}\mu\text{m}$ poling period. The second one is also a 500- μm thick PPLN, but the poling period becomes $\sim 30\text{-}\mu\text{m}$. The poling quality of the second PPLN sample is significantly worse than the first one, partly due to the increased difficulty in poling of smaller features. The domain size variation is too large to determine the duty cycle of this sample. We will soon demonstrate that with this poorly-poled sample, bulk SHG is observed in the non-poled domains, and serves as an indicator of poling quality. In order to confirm our observation is not due to PPC period, the poling period of the third sample is also close to 30- μm and the domain size is much more regular than the second one. The duty-cycle of the third sample is close to 50%, and the irregular domains only appear locally. The difference of the third sample is its 780- μm thickness, which may induce deviation of nucleation tips while poling, again resulting in bulk SHG within domains. The first sample can represent the normal SHG images of PPLN crystals, while the second and third samples provide different poling results with similar period for comparison. In the following section, we will demonstrate that the intensity of SHG signal inside domains, instead of at boundary, can be used as an indicator for poling quality.

4. Results and discussions

4.1 Well-poled PPLN

With optical sectioning capability of SHG microscopy, three-dimensional images are shown in Fig. 2. In the x-y section of Fig. 2(a), which is acquired in the middle of the PPLN crystal, the poled and non-poled domains are marked with arrows and arrow heads, respectively. The non-poled domain can be recognized by its direct connection with bulk LN in the center of the image. The duty cycle of this sample is close to 50%, and it is uniform over a few centimeters. Strong SHG is found only at the boundaries between poled/non-poled domains, agreeing well to previous observations [22–24]. Figure 2(b) gives quantitative SHG intensity distribution across three periods, manifesting that no SHG is observed within both poled and non-poled domains. Figure 2(c) shows two x-z sections from the same sample. The left picture, corresponding to the green dashed line in Fig. 2(a), is from the bulk LN area. Only surface SHG is seen in the x-z section, with diminishing bulk contribution. The result is consistent with our discussion for a z-cut bulk crystal in the last section.

On the other hand, the right picture of Fig. 2(c), corresponding to the red dashed line in Fig. 2(a), shows the x-z section of the PPLN area. The exceptionally regular periodic structure in all three dimensions demonstrates high-quality poling and reflects the uniform electric field distribution during the poling process. It is observed that the SHG at poled/non-poled

boundaries extends throughout the crystal but inside each domain, SHG is only generated at the upper and lower surfaces. This observation reflects that for a well-poled crystal, the optical axes of LN in poled/non-poled domains are parallel to the z axis, and thus no SHG is found within these domains.

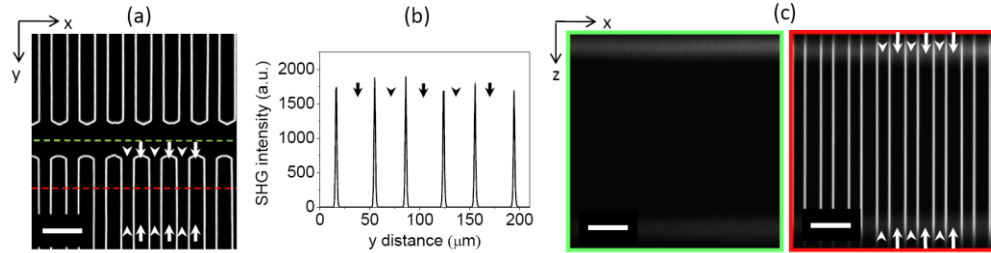


Fig. 2. SHG images of a well-poled PPLN. (a) is an x-y section at 280 μm depth from the sample surface. Arrows point out the poled domains while the arrow heads point out the non-poled domains. Scale bar: 100 μm (b) is the SHG intensity line profile across three periods showing that strong SHG is observed only at domain boundaries. (c) shows x-z sections of the bulk (left) and PPLN (right) areas, corresponding to the position of green and red dash lines in (a), respectively. Scale bar: 100 μm

4.2 Poorly-poled PPLN

Next, a 500- μm thick, poorly-poled PPLN with a ~ 30 μm period was examined, and the results are shown in Fig. 3. Representative x-y and x-z optical sections of the sample are shown in Figs. 3(a) and 3(b), respectively. Obviously, this sample is not as uniform as that in Fig. 2, both in x-y and x-z sections. Despite the sizes of electrodes are designed for a 50% duty cycle, the domain distribution is with large variation. In general, the widths of poled areas in this sample are larger than those of non-poled areas, and several merged domains or over-poled regions can be observed (red stars). Possible reasons for over-poling are excessive poling electric field or inadequate thickness of insulator.

Similar to the previously obtained results for the well-poled crystal, strong SHG is observed at boundaries between poled/nonpoled domains throughout the sample. However, apparent SHG within *non-poled* domains is found. For quantitative analysis, Fig. 3(c) shows the line profile of SHG intensities across three poling intervals. From Fig. 3(c), the clear separation between SHG of boundaries and SHG within domains manifests that the latter does not come from the former. The SHG intensity in the non-poled domain is significantly higher than that in the poled domain. This surprising result is somewhat counterintuitive, since non-poled area should exhibit the same properties as bulk crystal, where no SHG inside crystal is found when the ferroelectric polarization vector is perpendicular to the surface. One possibility is that due to the over-poling in this sample, a small tilt is induced in the polarization vectors of the non-poled domains. As a result, the nonlinear susceptibility tensor also rotates with the polarization vector. Therefore, the parts of the largest tensor element d_{33} can be accessed to generate bulk SHG emission. This assumption is reinforced by the observation that SHG in the non-poled domain is strongest when excitation-wave polarization lies in the x axis, which is the expected direction of tilt of SP under over-poling. It is interesting to notice that SHG intensity in the *poled* domains remains to be diminishing, suggesting that the polarization vector in the poled domain is still perpendicular to the surface. The relationship between over-poling and bulk SHG in the non-poled area will be addressed in more details in next subsection.

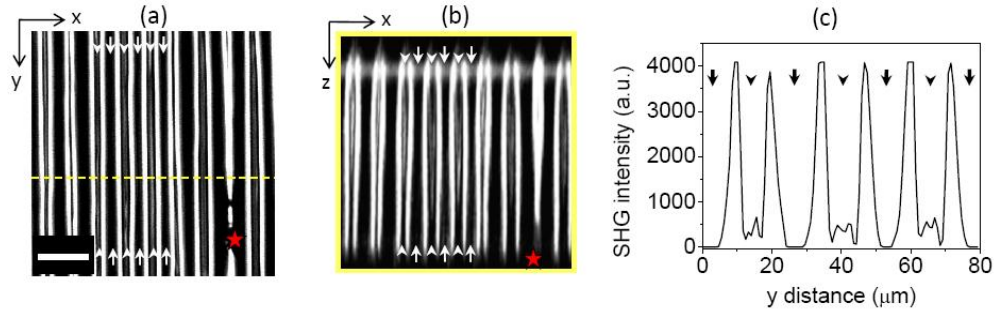


Fig. 3. SHG optical sections of a poorly-poled PPLN. (a) is an x-y section obtained at 300 μm from the sample surface. The poled and non-poled domains are marked with arrows and arrowheads, respectively. Scale bar: 50 μm . (b) is an x-z section corresponding to the position of yellow dashed line in (a). Red stars mark the merging of poled domains in x-y or x-z sections. The scale of x-axis is the same as (a), but for the sake of display, the z-axis in (b) is not in scale (sample thickness: 500 μm). (c) is the SHG intensity line profile across three poling periods showing SHG emission within the *non-poled* domains.

4.3 Moderate-quality PPLN

Figure 4(a) shows an x-y section of a 780- μm thick PPLN sample with a $\sim 30\text{-}\mu\text{m}$ period and a more uniform duty cycle. The image is taken at a depth of 390 μm below surface. Once again, strong SHG is found at poling boundaries, and SHG within domains is relatively weak. For the sake of description, two regions are highlighted in Fig. 4(b) and 4(c), and quantitative SHG intensities along several selected lines are provided in Fig. 4(d). It is interesting to notice that similar to Fig. 3, SHG within non-poled domains is observed, indicating that the poling was not perfect. But different from Fig. 3, SHG is observed in both poled and non-poled domains, and their intensities are comparable to each other. A possibility is that the SP of the LN wafer before poling is not perpendicular to the surface. But from the fact that there is no SHG in bulk LN area in Fig. 4, we suggest that SHG in both poled and non-poled domains is induced by poling process. Since the electric field modulation from electrodes would vanish in a distance similar to electrode separation, the propagation direction of nucleation tips can be easily deviant in a thick crystal, and subsequently the tilted SP induces SHG. This observation reflects the domain kinetics in thicker PPLN is more complex than thinner one, and more attention should be paid to electrode design for thick PPLN poling.

In Fig. 4(b), the widths of poled/non-poled domains are equal with parallel boundaries, suggesting an evenly distributed electric field during poling. As a result, the SHG intensity remains stable along the blue line in the non-poled domain, as shown by the blue curve in Fig. 4(d). The SHG in the poled domain is also constant within this region (data not shown).

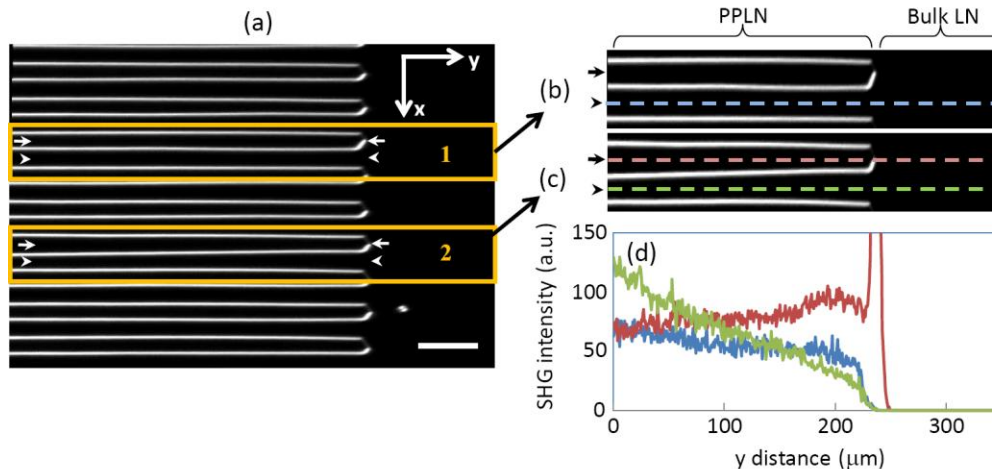


Fig. 4. (a) x-y optical section of a moderately-poled PPLN. Scale bar: 50 μm . (b) and (c) are enlarged portions of regions 1 and 2 in (a), respectively. Three different lines are selected, and their SHG line profiles are shown in (d).

In contrast, the widths of domains in Fig. 4(c) are slightly varied. In the non-poled area, the width is gradually widening from left to right, while the opposite is seen in the poled area. The non-parallel domain boundaries suggested irregular field distribution during poling. It is interesting to notice that within the poled domain, depicted by the red lines in Fig. 4(c) and 4(d), SHG intensity remains nearly unchanged. As mentioned, SHG in the poled area comes from the deviation of nucleation tips, so over-poling in the poled domain will not change the polarization vector, and SHG remains unchanged along the red line in Fig. 4(d).

Nevertheless, significant variation is found in the non-poled domain, as shown by the green lines in Fig. 4(c) and 4(d). At the region where the width of poled domain is larger, the SHG intensity in the non-poled domain also becomes larger. It can be readily explained by over-poling. The width broadening in the poled domain is caused by excessive poling electric field, which causes the crystal axis of adjacent non-poled domain to slightly rotate toward the poled domain, and therefore results in an increase of SHG. Again, the SHG in the non-poled domain is strongest when excitation polarization lies in the direction of crossing boundaries (x axis), reflecting the tilt orientation of SP.

Lastly, it is interesting to point that SHG drops to zero in bulk LN region in Fig. 4(d). As we have seen in Fig. 2 with a well-poled PPLN, SHG is also zero within both the poled and non-poled domains. Only when the poling condition is not ideal can the SHG within poled and non-poled domains be observed; that is, SHG intensity in the non-poled domains can be a quantitative diagnostic tool for poling quality, and it is a background-free measurement.

5. Summary and conclusion

It is known that SHG image is sensitive to nonlinear tensor orientation, and here we have demonstrated, for the first time, the application of bulk SHG microscopy to study poling quality in PPCs. To sum up, the schematics of normal and abnormal poling are plotted in Fig. 5. For normal poling condition in Fig. 5(a), the polarization vector is perpendicular to the crystal surface, and no SHG is observed inside the PPC. On the other hand, with excessive poling electric field in Fig. 5(b), the SP vectors of the non-poled domains can be slightly tilted toward the poled domains, while those of the poled domains remain to be perpendicular to the surface. The nonlinear susceptibility tensors in the non-poled domains rotate with the SP vectors, resulting in observable SHG. In addition, if PPLN is thicker, the propagation direction of nucleation tips is easily deviant. As a result, both poled and non-poled can be oblique, as shown in Fig. 5(c), and thus SHG can be found both in poled and non-poled domains.

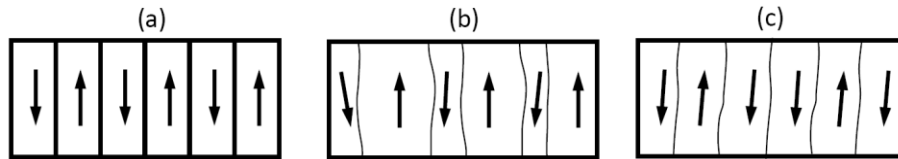


Fig. 5. Schematics of (a) normal poling, (b) over-poling, and (c) thick PPLN with both poled and non-poled are oblique. Arrows are ferroelectric polarization vectors.

The advantages of adopting SHG microscopy to study PPC includes intrinsic contrast without any special requirement on sample types or preparations, optical sectioning with sub-micrometer resolution, and deep observation capability. In the future, based on polarization anisotropy of SHG and combined with z-polarization analysis tools [30], detailed 3D orientations of ferroelectric polarization vector inside each domain can be extracted throughout the sample thickness, enabling SHG microscopy as a versatile and valuable tool to quantify the poling condition in PPCs.

Acknowledgments

We gratefully acknowledge the financial support of the National Science Council (NSC-98-2112-M-002-003-MY3, NSC 98-2738-M-002-001, and NSC98-2112-M-007-026), National Taiwan University (98R0321), and NTU Molecular Imaging Center. T.-M. Liu also wishes to acknowledge the support from NSC (NSC 99-2628-E-002-009), NHRI (NHRI-EX99-9936EI), NTU Frontier and Innovative Research Project (99R70411), and NTU Center of Genomic Medicine.